FISEVIER

Contents lists available at ScienceDirect

# Journal of Catalysis

journal homepage: www.elsevier.com/locate/jcat



Mini-review

# Catalysts and shape selective catalysis in the methanol-to-olefin (MTO) reaction



Jiawei Zhong <sup>a</sup>, Jingfeng Han <sup>a</sup>, Yingxu Wei <sup>a,\*</sup>, Zhongmin Liu <sup>a,b,c,\*</sup>

- <sup>a</sup> National Engineering Laboratory for Methanol to Olefins, State Energy Low Carbon Catalysis and Engineering R&D Center, Dalian National Laboratory for Clean Energy, iChEM (Collaborative Innovation Center of Chemistry for Energy Materials), Dalian Institute of Chemical Physics, Chinese Academy of Sciences, Dalian 116023, PR China <sup>b</sup> State Key Laboratory of Catalysis, Dalian Institute of Chemical Physics, Chinese Academy of Sciences, Dalian 116023, PR China
- <sup>c</sup> University of Chinese Academy of Sciences, 100049 Beijing, PR China

#### ARTICLE INFO

Article history: Received 27 October 2020 Revised 16 January 2021 Accepted 26 January 2021 Available online 4 February 2021

Keywords: MTO Shape selectivity SAPO Zeolites and molecular sieves

#### ABSTRACT

Recent advances in the shape selectivity of zeolites and molecular sieve catalysts for the methanol-toolefins (MTO) reaction are elaborated in this minireview. The concept and classification of shape selectivity are briefly introduced and summarized. The effect of cavity structure of cavity-type zeolites and
molecular sieves are comprehensively discussed, with focus on the formation of hydrocarbon pool intermediates, reaction route, diffusion, product selectivity, as well as deactivation in the chemical environment of cavity-type molecular sieves. Furthermore, the impact of topology of zeolites and molecular
sieves on reaction route and product selectivity are elucidated, with special attention on the shape selectivity of 1-dimensional 10-membered ring zeolites. The debate regarding the impact of coke formation on
product selectivity over SAPO-34 is also discussed in detail. Moreover, the progress of modification
strategies including metal cations incorporation and pre-coking process for improving shape selectivity
have been summarized. The perspective of shape selective catalysis in future is outlined and predicted.

© 2021 Published by Elsevier Inc.

#### 1. Introduction

In the past decades, due to the ever-increasing consumption of finite crude oil, the methanol-to-olefins (MTO) process has been developed and has become the most successful route for the production of value-added light olefin hydrocarbon products from abundant non-petrochemical feedstocks such as coal or natural gas [1–4]. The Dalian Institute of Chemical Physics (DICP) has been dedicated to the R&D of the MTO process for decades, and successfully developed the DMTO technology and realized the world's first commercialization of the MTO reaction in 2010. Afterward, DICP continued to develop the DMTO-II technology and completed the pilot test of the DMTO-III technology, so as to further increase the efficiency of light olefins production from methanol. For the formation of C—C bond-containing hydrocarbon products, the direct mechanisms may be operative in the initial stages of the reaction [5–7]. During the steady-state reaction stage, the indirect hydrocarbon pool (HCP) mechanism has been widely accepted for the formation of light olefin products, with aromatic carbenium ions, cyclic alkenyl ions, and the corresponding neutral species as the reactive HCP intermediates [8–10]. Light olefins are formed via acid-catalyzed cycles, such as the aromatics-based cycle, including side-chain methylation or paring routes, or the alkenes-based cycle with continuous alkenes methylation and cracking [11–15]. Recently, a cyclopentadienes-based cycle was proposed to run in parallel with the aromatics-based and alkenes-based cycles [16].

The alkanol transformations, typically exemplified by the MTO reaction, are catalyzed by microporous zeolites and zeotype molecular sieves [2,3,17,18]. Shape selectivity is a crucial property, which effectively discriminates zeolites and molecular sieves from other porous materials. In particular, shape selectivity of zeolite and SAPO molecular sieves is categorized into reactant shape selectivity, transition-state shape selectivity, and product shape selectivity [19].

It is widely accepted that the window dimensions of zeolite and SAPO molecular sieves have great impact on the product distribution due to the product shape selectivity. For example, a narrow 8-membered ring (8-MR) pore opening hinders the diffusion of aromatic molecules and branched hydrocarbons with high carbon numbers  $(C_nH_m, n > 4)$ , and achieves a high selectivity of  $C_2-C_4$  olefins of around 90%. In

E-mail addresses: weiyx@dicp.ac.cn (Y. Wei), liuzm@dicp.ac.cn (Z. Liu).

<sup>\*</sup> Corresponding authors.

particular, SAPO-34, silicoaluminophosphate (SAPO) molecular sieve with CHA topology is known as excellent catalyst for the selective formation of light olefins in the MTO reaction due to the structure with supercavities and 8-MR pore openings [11]. Moreover, the cavity structures and channel structures of zeolites and molecular sieves exert great influence on the reaction route and the formation of critical HCP species, thus control the product distribution in the methanol reaction via transition-state shape selectivity [20,21]. In addition, there has been a heated debate on the impact of coke formation and diffusion on product selectivity over SAPO-34, whether the product distribution variation with coke deposition is determined by transition-state shape selectivity or product shape selectivity [20].

The structure-performance relationship originates from the host-guest interaction of the MTO reaction system in the zeolite microenvironment. The host-guest interaction determines the formation of critical intermediates (HCP species), the energetically-feasible catalytic cycles with the detailed reaction routes, the formation of the product precursor and the ultimate product selectivity. The thorough understanding of the structure-performance relationship will effectively pave the way to a further optimization of the MTO catalyst and the MTO process. Therefore, in this minireview, we want to illustrate how shape selective catalysis controls the product generation in the MTO reaction. Studies discussing shape selectivity for methanol-to-gasoline (MTG) and methanol-to-aromatics (MTA) conversions are beyond the scope of this minireview.

#### 2. Shape selectivity of 8-MR and cavity-structured zeolite and zeotype catalysts

## 2.1. The formation of HCP species

According to the reaction mechanism of the MTO reaction, the indirect mechanism works as the efficient reaction pathway for the C—C bond-containing hydrocarbon products from the C1 reactant, methanol or dimethyl ether [12–15]. For 8-MR and cavity-type zeolites and molecular sieves, intensive studies indicated that the host cavity structures (e.g. size, shape, connectivity) determine the nature (structure and reactivity) of the critical HCP intermediates, thus control the olefin product distribution in the MTO reaction, based on the host-guest interaction of the catalytic system.

Liu's group investigated the correlation of HCP species formation and product generation during the MTO reaction, and revealed that confinement effects of host cavity determine the critical HCP intermediates and product distribution over 8-MR SAPO molecular sieves with different cavity structures [22–24]. The HCP intermediates formed in the MTO reaction catalyzed by the typical 8-MR and cavity-type SAPO and zeolite catalysts are summarized in Table 1. Under real MTO reaction conditions, polymethylbenzenium cations (polyMB $^+$ ) and polymethylcyclopentenyl cations (polyMCP $^+$ ) are directly observed by  $^{13}$ C solid-state NMR [23]. GC-MS analysis of the confined organics retained in the cavities after reaction at 300 °C shows that tetra-, penta-, and hexaMB are the dominant species over DNL-6 (RHO) and SAPO-34 (CHA), while tri-, tetra-, and pentaMB are predominantly formed over SAPO-35 (LEV) [23]. Their reactivity and role are further verified by the isotopic tracing method and theoretical calculations. Furthermore, the confinement effect from the cavity structure of SAPO-35, SAPO-34, and DNL-6 on product generation has also been analyzed. Butenes are mainly generated over DNL-6 (RHO cavity,  $11.4 \times 11.4$  Å), ethene and propene are main products over SAPO-34 (CHA cavity,  $6.7 \times 10$  Å), while ethene is predominantly generated over SAPO-35 (LEV cavity,  $6.3 \times 7.3$  Å). Although the 8-MR pore opening is very close for the 8-MR and cavity type SAPO molecular sieves, DNL-6, SAPO-34 and SAPO-35, the steric limitation imposed by the LEV cages results in the predominant production of ethene over SAPO-35 with the smallest cavity. Comparative studies indicated that the cavity size determines the molecular size and reactivity of confined HCP species as the critical intermediates, and in turn controls the MTO activity and product selectivity.

Recently, the methanol conversion over zeolite catalyst RUB-50 with LEV topology was studied as a case of host-guest interaction of the MTO reaction system. The impact of the small cavity on the HCP species formation and product distribution was investigated [24]. Higher ethene selectivity was also observed over RUB-50 than over other cavity-type catalysts including SAPO-34 [21], SSZ-13 (CHA topology) [9], and DNL-6 [10,23]. Methylbenzenium and methylcyclopentyl cations (triMCP+, triMB+, and tetraMB+) and corresponding deprotonated forms with less methyl groups were directly observed over H-RUB-50, in contrast to heptaMB+ and pentaMCP+ observed over SAPO-34 [23], SSZ-13 [9], and DNL-6 [8,10].  $^{12}$ C/ $^{13}$ C-methanol switch experiments confirmed the involvement of the intermediates triMCP, triMB, and tetraMB with fewer methyl groups in the methanol reaction over RUB-50. Theoretical calculations further confirmed that ethene and propene are generated by the energetically favourable side-chain methylation route rather than by the paring cycle.

Table 1
Carbenium ions formed in the MTO reaction over 8-MR zeolites and molecular sieves DNL-6 [8,10], SAPO-34 [9], SSZ-13 [9], SAPO-35 [23], RUB-50 [24], RUB-13 and ITQ-3 [25].

	Cavity	Size (Å)	SAPO	Zeolites
LEV		6.3  imes 7.3	Q-\$\langle\$	\$\dop
СНА		6.7 × 10	\(\frac{1}{2}\)	<b>以</b>
RTH		9.8 × 13.8		¥
ITE		9.8 × 13.8		Ť
RHO		11.4 × 11.4	**	

Corma et al. investigated the impact of cavity structure on the relative stability of MB+ intermediates involved in the paring and sidechain methylation routes. They revealed that the degree of methylation of the MB+ cations strongly correlates with the product distribution. The preferential stabilization of partly methylated penta-MB+ in SSZ-13 (CHA) initiates the side-chain methylation pathway, thus favoring the production of ethene. By contrast, the preferential stabilization of the fully methylated heptaMB<sup>+</sup> in RUB-13 (RTH) and ITQ-3 (ITE) benefits the paring route, thus facilitating the generation of propene and butenes [25]. More recently, their theoretical calculation work suggested that cavity topology and its ability to preferentially stabilize the fully methylated 7 MB+ cations is the key factor controlling product distribution, as confirmed by the linear relationship between the experimentally determined  $C_3^*/C_2^*$  ratio in CHA and AEI structures (SSZ-13, SAPO-34, SSZ-39 and SAPO-18) and the  $E_{int(7/5)}$  parameter, the interaction energy ratio of 7 MB<sup>+</sup> and 5 MB<sup>+</sup> [26].

# 2.2. Product selectivity

Intensive studies paid great attention on the effect of cavity structures on product selectivity due to the application of this kind of materials as industrial catalyst. For example, Gascon *et al.* reported that ethene, propene, and linear butenes are generated with high selectivity, and no hydrocarbon products higher than  $C_4$  olefins are formed over ZSM-58 (DDR) [27]. Anderson *et al.* reported the ratio of ethene to propene is strongly correlated to the cavity structures, and suggested that SAPO-34/SAPO-18 intergrowth with high AEI content provides low ratio of ethene to propene, and high selectivity to propene and butene [28]. Pinilla-Herrero *et al.* investigated the effect of framework topology of SAPO-35 (LEV), SAPO-56 (AFX), STA-7 (SAV), and SAPO-42 (LTA), and found that the size and shape of cavities and 8-MR pore openings influence the product distribution [29,30]. Ethene and propene were mainly generated over SAPO-35, SAPO-56, and STA-7. The highest ethene selectivity was obtained over SAPO-35 with smallest LEV cavities, while  $C_4$  olefins were predominantly produced over SAPO-42 with larger LTA cavities. In particular, though with larger and elongated AFX cavities, SAPO-56 also catalyzes the major formation of ethene and propene from methanol conversion, due to the small size of the 8-MR windows (3.6  $\times$  3.4 Å), indicating that the size of the pore openings also plays an important role in the product distribution [31].

A systematic and comprehensive analysis was carried out by Davis and co-workers to reveal the effect of cavity structure of zeolite catalysts on the product selectivity in the MTO reaction [31–34]. For example, with similar Si/Al ratios and crystal sizes, the MTO performance of 8-MR zeolites with different cavity structure (LEV, CHA, AFX) was compared [32]. The reaction performed over catalysts with smaller cavity size generated more ethene product among the light olefins. Among all the 8-MR and cavity-type catalysts, the highest ethene selectivity was obtained over the smallest LEV structure, and the maximum propene selectivity was obtained over zeolites with CHA structure. Furthermore, based on the observations of product distribution over a series of small-pore zeolites, the MTO-active topologies were classified into four types based on the light olefin distributions at 400 °C: 1) the ethene and propene selectivities are roughly equal and the butene selectivity is low over catalysts with CHA, AFX, SFW, and GME-related ABC-6 family topologies, 2) the ethene selectivity is higher than that of propene and the butene selectivity is low over zeolites with cavities of LEV, ERI, or ERI-related intergrowth, 3) the propene selectivity is higher than that of ethene, with butene selectivity similar to that of ethene over zeolites with cages wider than CHA (e.g. AEI, DDR, RTH, ITE), 4) the ethene, propene, and butene selectivities are roughly equal over zeolites with wide *lta*-cavities (LTA, RHO, KFI) [33].

More recently, Davis and co-workers proposed the novel ellipsoidal model with cage-defining ring and cage-defining ring size. As shown in Fig. 1(a), 1(b), the ellipse ab is defined as the cage-defining ring of the ellipsoidal cage, and the length of axis b that limits the maximum size of the polymethyl-aromatic intermediates within the cages is denoted as the cage-defining ring size. A relationship between the cage-defining ring size and the light olefin product distributions was established (Fig. 1(c)) [34]. As shown in Fig. 1(c), the cage structures are classified into the following four types based on the cage-defining ring size. 1) ethene selectivity close to propene over zeolites with CHA, AFX, and SFW containing 12-membered cage-defining ring with almost the same ring size of 7.45 Å. 2) higher ethene than propene selectivity over zeolites containing 12-membered cage-defining rings with sizes smaller than 7.45 Å (LEV, ERI). 3) higher propene selectivity than that of ethene over zeolites with wider 14-membered cage-defining rings except for DDR. 4) high butene selectivity over zeolites possessing widest 16-membered cage-defining rings with ring sizes>10 Å. This classification relates the product formation to the structure and size of the cages, while the chemical origin and intrinsic mechanism of the cage-defining ring and cage-defining ring size have not been considered together.

It was found that beside the cavity size related hydrocarbon pool species formation, the host cavity structures would also exert great impact on the reaction route (aromatics-based cycle or alkenes-based cycle), thus determine the ultimate product distribution. Recently, It is found that SAPO-14 with AFN topology and ultra-small cages  $(5.3 \times 10.5 \text{ Å})$  exhibits an unprecedentedly high propene selectivity of 77.3%. Combined isotopic switch experiments and reaction-diffusion simulations demonstrated that the olefins-based cycle dominates the MTO reaction, with the aromatics-based cycle being suppressed. The unique AFN topology with ultra-small cages, combined with

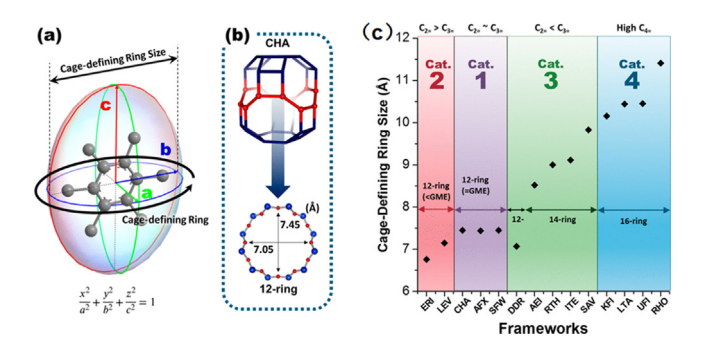


Fig. 1. (a) An ellipsoidal model for the cage-defining ring and the cage-defining ring size. (b) The selection of the cage defining ring from a CHA-cage. (c) Correlation chart of cage-defining ring size by cage structures and light olefin product distribution categories. Modified on Ref. [34] with permission from Ref. [34].

the low acid concentration, contributes to the olefins-based cycle and facilitates the propene generation. Meanwhile, the narrower 8-MR pore opening limits the diffusion of  $C_{4+}$  products, thus results in the high propene s electivity [35].

# 2.3. Diffusion

In addition to the confinement effect on the formation of HCP intermediates, the predominant reaction route, the confinement or restriction caused by cavity structure also influences the diffusion of guest molecules, and contributes to the product shape-selectivity [36,37]. Recently, Liu's group investigated the diffusion behavior of guest hydrocarbons within confined environment, and revealed the diffusion behavior in cavity-type molecular sieves [38]. The self-diffusion coefficients of alkanes within cavity-type molecular sieves, obtained from pulsed field gradient (PFG) NMR and molecular dynamics simulations, decreased in the order DNL-6 (RHO) > SAPO-34 (CHA) > SAPO-35 (LEV). In addition, jump frequency and jump length, obtained from the continuous-time random-walk coarse-graining method, have been adopted to quantitatively depict the inter-cavity hopping process (Fig. 2). The lower restriction from the large *lta* cavity and the long distance between adjacent sites lead to the high jump frequency and long jump length in the RHO molecular sieve, while the strong confinement of the LEV cavity and short distance of adjacent cavities result in the lowest diffusion coefficient with low jump frequency and short jump length.

#### 2.4. Deactivation

The cavity-type zeolite and zeotype catalysts with small 8-MR window encounter deactivation caused by the aging of the retained coke species. Cavity structures determine the coke species confined in the cavities, with the carbonaceous deposits presenting with bulky size. The aromatic condensation to bulky polycyclic aromatics causes catalyst deactivation, accompanied by the additional propane formation. Davis *et al.* reported that the initial propane selectivity is related with the dimension of the zeolite cage [33]. For a given Si/Al ratio, the larger the cage dimension, the higher the propane selectivity and the shorter the catalyst lifetime. The initial propane selectivity follows the order AFX, SFW > AEI, RTH, LTA, RHO > CHA > LEV, ERI. In contrast to zeolites with CHA cavities, zeolites with larger cages generate bulky organics more easily and suffer from quick deactivation.

Recently, thanks to the integration of advanced MALDI FT-ICR mass spectrometry with isotope labeling technique, a novel "aromatic cage-passing" deactivating mechanism was unveiled in SAPO-34-catalyzed MTO process [39]. Wherein, three- to four-ring aromatic hydrocarbons, which are primarily formed in CHA cages, function as the coking "building block". With reaction going, they traverse the 8-MR windows of CHA cages and are being cross-linked with the neighboring coking unit, leading to the interconnected multicore aromatics. This "aromatic cage-passing" mechanism was also applicable to other cage-structured zeolites such as SAPO-18 and SAPO-35 (Fig. 3). The distinction lies in the chemical nature (or dimensions) of the coking unit which varies with the cavity sizes of zeolites. These findings arrive at a conclusion that coking/deactivating in cavity-type zeolite and zeotype catalysts is a cavity-controlled process characterizing shape-selective feature.

# 3. Shape selectivity from the topology of zeolites and molecular sieves on reaction route and product selectivity

In general, the formation of HCP intermediates can only take place in zeolites and molecular sieves with spacious cages or intersectional channels. Therefore, in addition to the cavity structures of cavity-type zeolites and molecular sieves, the topology of zeolites and molecular sieves also influences the accommodation and stabilization of the critical HCP species. In addition, the topology of zeolites and molecular sieves exerts great impact on the reaction route, thus affecting the ultimate product selectivity in the MTO reaction.

In addition to the 8-MR cavity-type zeolites and molecular sieves discussed above, medium-pore 10-MR zeolites and molecular sieves composed of straight and/or curved channels have also been widely investigated. The shape/size/reactivity of the active HCP species depend on the dimensions of the channel intersection, which is similar to the findings for the cavity-type 8-MR molecular sieves [4]. For the 3-dimensional MFI structure with intersectional sinusoidal  $(5.1 \times 5.5 \text{ Å})$  and straight  $(5.3 \times 5.6 \text{ Å})$  channels, the "dual-cycle" mech-

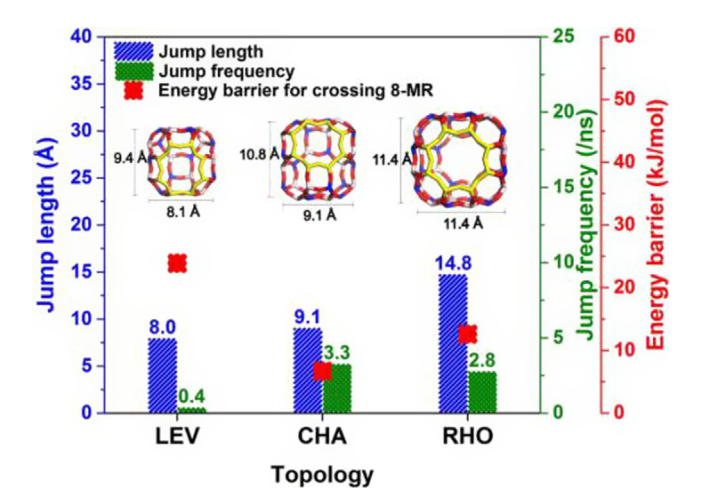


Fig. 2. The average jump frequency and jump length of methane in LEV, CHA, and RHO and the corresponding energy barrier for crossing 8-MR of methane in the inter-cavity hopping process. Reproduced with permission from Ref. [38]. © 2019 Elsevier Inc.

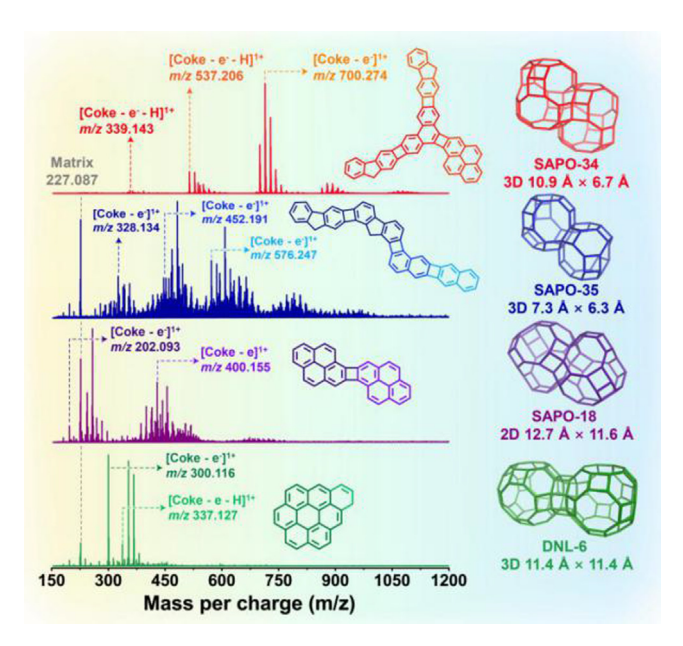


Fig. 3. Molecular structure analysis of deactivating species in cage-structured molecular sieves by MALDI FT-ICR mass spectra. Reproduced with permission from Ref. [39].

anism is widely accepted for MTH reaction over ZSM-5, with ethene and propene generated via an aromatics-based cycle and  $C_3^*$  alkenes generated via an olefins-based cycle, namely, an olefin methylation-cracking route [40,41]. The manipulation of the prevalence of certain reaction cycles (aromatics-based/olefins-based cycle) can further tune the selectivity for specially required hydrocarbon products from methanol conversion, such as MTO reaction for the production of ethene and propene or MTP reaction for the production of propene as the main product.

1-dimensional 10-MR zeolites have attracted particular interest in past years. Due to the 1-dimensional 10-MR straight channels in TON topology (4.6 Å  $\times$  5.7 Å), high selectivity towards  $C_{5+}$  aliphatics is obtained over ZSM-22, and the olefin methylation-cracking route is generally accepted as the main route for the product formation over ZSM-22 [42–44]. However, the formation of methylcyclopentenyl cations (MCP<sup>+</sup>) and the deprotonated counterparts were identified in the induction period, thus the HCP mechanism cannot be ruled out over H-ZSM-22, especially at the very beginning of the reaction, although the alkene methylation-cracking route acts as the main route [45].

Svelle and co-workers compared the product selectivity of 1-dimensional 10-MR zeolites including ZSM-22 (TON, 4.6 Å × 5.7 Å), ZSM-23 (MTT, 4.5 × 5.2 Å), ZSM-48 (MRE, 5.6 × 5.3 Å), and EU-1 (EUO, 5.4 × 4.1 Å). The ZSM-22 and ZSM-23-catalyzed reaction displayed high selectivity toward the non-aromatic  $C_{5+}$  hydrocarbons, while over ZSM-48 with relatively larger pore size and EU-1 with narrower pore size but 12-ring side pockets on the outer surface, the methanol reaction generated substantial amounts of aromatics in the  $C_{5+}$  fraction [46]. The shape selectivity of one-dimensional 10-MR zeolites ZSM-22 (TON), ZSM-23 (MTT), ZSM-48 (MRE), EU-1 (EUO), two-dimensional zeolite Ferrierite (FER), ZSM-57 (MFS), and three-dimensional molecular sieves SAPO-34 (CHA), SUZ-4 (SZR), and ZSM-5 (MFI) was comprehensively studied [11,47]. 10-MR zeolites ZSM-22, ZSM-23, and Ferrierite yielded hydrocarbon products rich in  $C_{5+}$  hydrocarbons and nearly free of aromatics, while ZSM-57, EU-1, and ZSM-48 yielded hydrocarbon mixtures rich in aromatics, similar to that observed over ZSM-5, due to the fairly large 10-MR of MRE and MFS, the large side pockets of EUO, respectively. In particular, similar to SAPO-34, SUZ-4 displayed high selectivity toward  $C_2$  and  $C_3$  hydrocarbons. SUZ-4 crystals exhibit needle-like morphology, with 8-MR and 10-MR channels oriented perpendicular and along the needles, respectively. The 8-MR channels dominate and control the product distribution and result in a morphology-induced shape selectivity [47].

10- and 12-MR zeolite and molecular sieves achieving high selectivity to  $C_3$ - $C_4$  olefins have also attracted great interest [48–50]. For example, CON-type zeolites consisting of 3D pore system with 12-, 12-, and 10-MR pores, exhibited low ethene selectivity, high propene selectivity and high C3-C4 selectivity of 80% in MTO reaction [48]. Similarly, 3D MCM-68 zeolite with 12-, 10-, 10R channel system (MSE-type) exhibit low selectivity for ethylene and high yields of propylene and butylenes in dimethyl ether-to-olefins (DTO) reaction [49–50]. Recently, Liu's group found that high-Si beta exhibited high propene selectivity and propene/ethene ratio, due to the dominated olefin-based mechanism contributing to the formation of ethene, propene, and higher olefins [51,52].

As for other large-pore 12-MR zeolites and molecular sieves such as faujasite (FAU), aromatics can easily flow out as the effluent products, and higher selectivity to aromatics are generally obtained, which make it far from a satisfactory catalyst for the methanol-to-olefins reaction, and will therefore, not be discussed in this minireview.

# 4. Effects of coke formation and diffusion limitation over SAPO-34 on shape selectivity

With the proceeding of the MTO reaction over cavity-type zeolite or molecular sieve catalysts, such as SAPO-34, the transformation of confined HCP species in the CHA cavities into cross-linked multicore polycyclic aromatic hydrocarbons with graphene-like structure via cage-passing growth, suppresses the mass transfer, makes the reaction centers inaccessible to the reactant, and leads to quick catalyst deactivation [11,39]. In general, the ethene selectivity and ethene-to-propene ratio increase and the selectivities to propene and  $C_4$ - $C_6$  molecules decrease with the coke deposition over SAPO-34, reflecting the pronounced shape selectivity variations [53–57]. The optimal selectivity to light olefins at high methanol conversion (>99%) is favored with certain coke content, therefore, in the industrial application,

a fluidized-bed reactor is adopted to solve the deactivation problem and achieve steady-state performance with a constant coke content [1]. However, there are longstanding controversies whether the selectivity of  $C_2$ - $C_4$  olefins over SAPO-34 in the MTO reaction is governed by the generation and involvement of HCP intermediates, the transition-state selectivity, or product shape selectivity [54].

On one hand, some scholars proposed that the decrease in the free space in the cavities with rising coke amount inhibits the formation of specific HCP species, thus favoring ethene generation. Song *et al.* reported that the selectivity of light olefins over SAPO-34 is correlated with the number of methyl substituents of MB trapped in the nanocages. Ethene formation is favored by the participation of xylenes and triMB as the HCP species, while propene generation is favored by tetra- to hexaMB as the critical intermediates [58]. Later, through in situ <sup>13</sup>C MAS NMR and UV/Vis spectroscopy, Hunger *et al.* proposed that a decrease of the mean number of methyl groups per aromatic ring of HCP species with deactivation is responsible for the change of the product selectivity from propene to ethene over SAPO-34 [59].

On the contrary, Barger measured the distribution of  $C_2$ – $C_5$  olefins generated at different temperatures. He observed a higher ethene-to-propene ratio than that calculated from thermodynamic equilibrium, and concluded that equilibration of ethene and propene is established prior to diffusion out of the pore structure. The propene diffusion is hindered relative to that of ethene, and product distribution over SAPO-34 is governed by product shape selectivity [54]. Olsbye *et al.* conducted isotopic switch experiments ( $^{12}C/^{13}C$  methanol) over active, partly deactivated, and severely deactivated SAPO-34 catalysts and found that the  $^{13}C$  fraction in the retained MB intermediates decreased in the order: hexaMB > pentaMB > tetraMBs > triMBs > xylenes > toluene. They concluded that the increase in ethene selectivity with time on stream was attributed to the pore clogging and diffusion hindrance of propene and the higher alkenes, namely, the product shape selectivity [56]. Via a combination of in-situ UV/Vis spectroscopy and confocal fluorescence micro-spectroscopy, Weckhuysen *et al.* confirmed that the fluorescent aromatic species mainly remain located at the near-surface region of SAPO-34 crystals with time-on-stream, thus hindering the diffusion through crystals, leading to the decreased accessibility of crystal internal region to reactant molecules, and ultimate catalyst deactivation [60].

In particular, Liu's group has conducted comprehensive study on evolution of molecules and active sites, and the role of coke formation and diffusion of SAPO-34 in the MTO reaction. For example, it is found the location, amount, and size of coke species confined in the CHA nanocages exerted great impact on the deactivation of the catalysts [61]. The nonuniform spatial distribution of coke species with yolk-shell-like structure was confirmed by confocal fluorescence microscopy, while the loss of micropore volume was probed by hyperpolarized <sup>129</sup>Xe NMR. On one hand, the occupation of the cavities in the shell layers of the crystals by bulky coke species resulted in a decrease in the intracrystalline mass transport, as indicated by the declined self-diffusion coefficient and the increased diffusion activation energy obtained by PFG NMR. On the other hand, as indicated by DRIFT, the nonuniform spatial distribution of coke species with yolk-shell-like structure also caused the accessibility loss of the Brønsted acidic sites in the inner parts of the crystals. The nonuniform coke formation in the crystals, the decreased intracrystalline mass transport behavior, and the decreased number of accessible Brønsted acidic sites with coke deposition result in the deactivation of SAPO-34 catalysts in the MTO reaction.

More recently, ever-increasing interest have been focused on in situ techniques to delve into the impact of coke and diffusion limitation. Liu's group performed a real-time investigation of the methanol conversion and the molecular diffusion behavior in SAPO-34 catalysts via a pseudo-gas chromatography method, and quantitatively interpreted the role of diffusion in methanol conversion, deactivation, and product selectivity [62]. Methane, ethane, propane, and isobutane were adopted as the probe molecules, representing the diffusion of reactant and products. In the whole course of the MTO reaction, methane passes through the catalyst bed with sole intracrystalline diffusion mode, whereas isobutane passes through the catalyst bed with the intercrystalline diffusion mode. Ethane maintains the dominant intracrystalline diffusion mode before deactivation, while propane presents the dominant intercrystalline diffusion and intracrystalline diffusion is depressed with time on stream (Fig. 4). Therefore, the diffusion-related shape selectivity was clearly elucidated. The catalyst deactivation is ascribed to the accessibility decrease of the catalyst microporous surface for methanol, which is closely related to the reactant diffusion in the microporous catalyst with continuous coke deposition. The increased selectivity to light olefins and the increased ratio of ethene to propene with time on stream is ascribed to the enhanced intracrystalline diffusion limitation for large hydrocarbon products.

In addition to the intracrystalline diffusivity that is mainly determined by the topological structure of host materials and the steric dimension of guest molecules, some recent study indicates the role of surface barrier in the mass transport of guest molecular. The surface permeability is sensitive to the non-ideality of a crystalline surface due to the physical and chemical properties and host-guest interaction at crystalline surface [63]. Furthermore, by the aid of combined multi-scale reaction-diffusion simulation with high-resolution structured illumination microscopy (SIM), Liu's group investigate the spatiotemporal evolution of gas molecules, carbonaceous species and the active sites at individual SAPO-34 crystal scale in MTO reaction [64]. It is found that the crystal size, i.e., diffusion length, predominantly determines the accessibility of acid sites, evolutions, spatial distribution of carbonaceous species, and diffusion of gas molecules during MTO

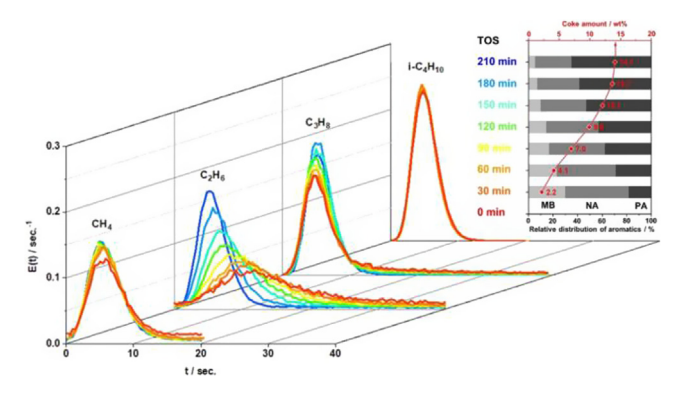


Fig. 4. Experimental RTD curve of CH<sub>4</sub>, C<sub>2</sub>H<sub>6</sub>, C<sub>3</sub>H<sub>8</sub>, and i-C<sub>4</sub>H<sub>10</sub> probing on the SAPO-34 catalyst bed during the MTO reaction. Inset: coke amount and distribution. MA, NA, and PA represent methyl-substituted benzenes, naphthalenes, and polyaromatics, respectively. Reproduced with permission from Ref. [62].

reactions. Shorting the diffusion pathway facilitates methanol to diffuse into the center of crystals and make higher utilization of acid sites inside crystal, beneficial for the diffusion of gas product formed inside crystal toward the rim of crystal. The rapid catalyst deactivation is mainly caused by the deposition of coke precursors at the crystal rim.

Similarly, Speybroeck *et al.* deeply analyzed the impacts of temperature, Brønsted acid sites, micro-environment with HCP species in catalyst and methanol on the diffusion behavior of light olefins through the 8-MR windows of SAPO-34, via enhanced sampling molecular dynamics simulations based on force fields or density functional theory. In particular, the nature and spatial distribution of the HCP species substantially affects the diffusivity of light olefins. Ethene and propene will be expelled immediately from a cage containing HCP species (e.g. hexaMB) to a neighboring cage without bulky HCP species. The continuous generation and accommodation of bulky HCP species and coke species severely hinder the diffusion, and result in the change in product distribution with time on stream [65].

The molecular diffusion in zeolite channel is a shape-selective process. As discussed above, MTO reaction exhibits the dynamic coking behavior, wherein the evolving mass growth of coking species appreciably affect the molecular transport and then progressively sieve the lighter olefins, especially ethene, as the main product [11,39]. The benefits of coking on product selectivity control inform the MTO industrial strategy to effectively modulate the product selectivity.

# 5. Modification strategies for the achievement of shape selectivity

In order to vary the product selectivity for the generation of specially required olefins and optimize the selectivity to light olefins, a variety of strategies has been developed. Song et al. modified the CHA nanocages in SAPO-34 via a ship-in-bottle synthesis from PH<sub>3</sub>, and the introduction of phosphate species decreased the volume of the nanocages and improved the ethene selectivity [66]. In addition, it was revealed that the cavity modification via diffusion property adjustment can effectively steer the selectivity toward a certain demanded olefin product. Recently, an effective way to manipulate the light olefin selectivity based on the development of SAPO-34 or SAPO-18 catalysts modified with zinc cations was proposed, and the relationship of "metal cations incorporation-reaction environment modificationadjustment of reaction and diffusion property" was revealed [67–70]. Since the exchanged zinc cations are mainly located in the subsurface of the SAPO catalysts, the Si-enrichment at the periphery of SAPO-34 and SAPO-18 catalysts leads to more ion-exchangeable acid sites in the layer near the external surface, thus more zinc cations were incorporated into the more acidic cavities in the Si-enrichment layer. Both the zinc cations accommodation in the cavities of the shell layer and the facilitated formation of bicyclic aromatics over the catalysts modified with zinc cations with a core-shell-like structure increase the diffusion hindrance for bulky hydrocarbons. Meanwhile, lower methylbenzene and methylnaphthalene intermediates that favor the ethene generation are more predominant over catalysts modified by zinc cations, leading to an enhanced ethene selectivity and ethene-to-propene ratio in the initial reaction stage of methanol conversion [67]. Higher selectivity to light olefins is achieved over zinc cation-modified SAPO-34 or SAPO-18 at shorter contact time and with a relatively lower coke amount, compared with the unmodified counterparts. However, the catalyst lifespan is slightly shortened over zinc cationmodified SAPO-34 or SAPO-18 [68,69]. Furthermore, a novel template-assisted ion incorporation method, based on the interaction between zinc cations and the nitrogen atom of the template, has also been developed [70]. The zinc cations were introduced into the as-synthesized SAPO molecular sieves without the removal of template by calcination. The nitrogen atoms in the template function as the anchoring sites for the zinc cations. After the introduction of zinc ions, the template was removed by calcination and the zinc cations are stabilized at the ion-exchangeable acid sites, and modified catalysts with relatively enriched Zn cations in the sublayer near the external surface are obtained ultimately. Enhanced selectivity to ethene and light olefins are obtained at the beginning of the reaction over SAPO-34 modified with zinc cations by the template-assisted ion incorporation method. Similarly, an enhanced ethene-to-propene ratio has also been obtained over Zn-modified SAPO-34 prepared by the impregnation method. This is ascribed to the increased diffusion limitation originating from the Zn-related species enrichment and the facilitated formation of aromatics in the cavity-type molecular sieve catalysts [71,72].

More recently, the controlling of surface barriers in SAPO-34 is reported to exert great impact on the light olefins selectivity and the catalyst lifespan [73]. Through chemical liquid deposition (CLD) and acetic acidic etching, the surface properties was successfully modified, while the morphology, internal structure and acid properties of SAPO-34 were maintained, thus the surface permeability was regulated and the intracrystalline diffusivity was maintained. The decrease of surface barriers leads to prolonged catalyst lifetime and promoted light olefins selectivity.

In practical MTO industry, partial regeneration technology for the deactivated catalyst and pre-coking technology for fresh catalysts are typical industrial technologies to increase the lower olefin selectivity in the initial reaction stage. Liu's group developed pre-coking technology in which coke species were preformed and located in the cavity-type catalysts while conducting 1-butene conversion over SAPO-34. This enhanced the ethene selectivity remarkably while the catalyst lifetime was maintained [74]. Combined  $^{12}$ C/ $^{13}$ C-methanol switch experiments, MD calculations, and FTIR analysis demonstrated that the enhanced ethene selectivity can be attributed to the spatial location of the pre-situated "coke" instead of simply or solely to the configurational diffusion effect, the transition-state shape selectivity, or the co-catalysis of methylnaphthalene species. The relatively even distribution of pre-situated coke by 1-butene precooking extends the reaction zone inward in the inner part of the SAPO-34 crystals, enhances the utilization efficiency of Brønsted acid sites, and prolongs the diffusion length of molecules. The diffusion-hindered higher olefinic species tend to evolve to active aromatic species and facilitate the ethene generation.

# 6. Conclusions and outlook

In this minireview, the influences of cavity structure and topology of zeolites and molecular sieves on the formation of critical HCP intermediates, reaction route, and ultimate product distribution in the MTO reaction have been analyzed. The impact of coke formation and diffusion on product selectivity has been discussed. Novel modification strategies for shape selective catalysis have also been illustrated. We hope that this minireview will provide deeper understanding of the shape selective catalysis of zeolites and molecular sieves in the MTO reaction. The catalyst development and reaction mechanism studies for the MTO reaction improve the shape-selective catalysis including the modulation of the formation of reaction intermediates, the selection of detailed reaction paths, the accumulation of coke deposits, and the diffusion feasibility. All these reflect the unique shape selectivity of molecular sieve and the unique dynamic reaction

characteristics of the methanol conversion reaction. Further understanding of the structure-performance relationship relies on combined and advanced techniques, such as in situ techniques (\frac{13}{C}\text{ NMR spectroscopy, FTIR spectroscopy, UV/vis spectroscopy, electron spin resonance, etc.) for the observation and characterization of the critical reaction intermediates, PFG NMR spectroscopy and neutron scattering technology for the research of the diffusion behavior of guest hydrocarbons within confined environment, isotopic labelling experiments for the identification of reaction pathways, as well as theoretical calculations for simulations.

For MTO process, the realization of shape-selective catalysis performance with improved reaction efficiency is the goal of the development of next-generation catalyst. The priority of catalyst development is to efficiently synergize indirect reaction mechanism, coke deposition, and diffusion limitation, so as to promote the shape-selective catalysis. Both the rational catalysts design and shape-selective strategy with precise control are critical directions for future academic and industrial research. Light olefins with specific distribution in ethene, propene and butenes are the target products of the conventional MTO process. In response to the varied demand in the international olefin market, it is highly desirable to steer the selectivity to realize the processes such as MTE (methanol-to-ethene) and MTP (methanol-to-propene). For example, high-silica silicoaluminates, including ZSM-5 and beta [51,52], have been developed to maximize the propene production. In particular, DICP successfully developed the fluidized-bed DMTP technology for propene production over SAPO-based catalyst, by coupling three reaction processes including methanol conversion, alkylation of ethene by methanol, and C<sub>4+</sub> cracking processes. The development of the catalyst and the reaction process that matches the catalytic behavior will be the key to the development of a specific process for required olefin product.

Furthermore, by contrast to the commercial two-process route consist of *syn*-gas to methanol and consecutive MTO process, the direct conversion of CO and CO<sub>2</sub> to lower olefins has become a hot research direction in C1 chemistry [75,76]. For the direct *syn*-gas conversion to lower olefins, the selectivity of light olefins via typical Fischer-Tropsch (FT) synthesis (known as FTO route) is limited by the Anderson-Schulz-Flory (ASF) distribution, thus great interest have been focused on the single-pass non-FT process via ketene/methanol/DME intermediate over tandem catalysts consist of metal oxide (ZnCrO<sub>x</sub> [77], ZnAlO<sub>x</sub> [78], ZnO-ZrO<sub>2</sub> [79,80], etc.) and molecular sieves with CHA topology (SAPO-34, SSZ-13, etc.). As for the CO<sub>2</sub> conversion to lower olefins via methanol/DME intermediate, bifunctional catalysts composed of metal oxide (ZnO-ZrO<sub>2</sub> [81], In<sub>2</sub>O<sub>3</sub>-ZrO<sub>2</sub> [82], etc.) and molecular sieves (SAPO-34, Zn-modified SAPO-34, SSZ-13, etc.) are also adopted. For the light olefins synthesis from the direct CO and CO<sub>2</sub> conversion, the selectivity of ultimate product is also highly determined by the shape-selective catalysis of molecular sieves. However, until now, no deep investigations have been devoted to the detailed mechanisms and kinetics of for CO and CO<sub>2</sub> conversion into lower olefins over the metal oxide/molecular sieves bifunctional catalysts, the presence of CO, CO<sub>2</sub>, and H<sub>2</sub> complicate the shape-selective catalysis and reaction mechanism, and may even alter the species, reaction pathways as well as the diffusion behaviors inside the CHA cavity of molecular sieves, thus in-depth experimental studies and DFT calculation are still of great significance and necessities to elucidate the exact mechanism of the conversion of methanol/DME intermediate to light olefins in the presence of CO, CO<sub>2</sub>, and H<sub>2</sub>, and to classify the difference to the widely-accepted HCP mechanism for the MTO reaction.

# **Declaration of Competing Interest**

The authors declare that they have no known competing financial interests or personal relationships that could have appeared to influence the work reported in this paper.

# Acknowledgements

The authors highly appreciate the insightful supplement and polish from Dr. Yuchun Zhi and Dr. Mingbin Gao as well as the thorough discussions with Dr. Wenna Zhang, Dr. Shanfan Lin and Dr. Shushu Gao. The authors are also grateful to the National Natural Science Foundation of China (21603223, 91745109, 91545104, 21473182, 91334205, 21703239) and the Youth Innovation Promotion Association of the Chinese Academy of Sciences (2014165) for financial support.

# References

- [1] P. Tian, Y.X. Wei, M. Ye, Z.M. Liu, ACS Catal. 5 (2015) 1922-1938.
- [2] S.T. Xu, Y.C. Zhi, J.F. Han, W.N. Zhang, X.Q. Wu, T.T. Sun, Y.X. Wei, Z.M. Liu, in: Advances in Catalysis, Academic Press, 2017, pp. 37–122.
- [3] J.W. Zhong, J.F. Han, Y.X. Wei, P. Tian, X.W. Guo, C.S. Song, Z.M. Liu, Catal. Sci. Tech. 7 (2017) 4905–4923.
- [4] M. Yang, D. Fan, Y.X. Wei, P. Tian, Z.M. Liu, Adv. Mat. 7 (2019) 1902181.
- [5] Y. Liu, S. Muller, D. Berger, J. Jelic, K. Reuter, M. Tonigold, M. Sanchez-Sanchez, J.A. Lercher, Angew. Chem. Int. Ed. 55 (2016) 5723–5726.
- [6] X.Q. Wu, S.T. Xu, W.N. Zhang, J.D. Huang, J.Z. Li, B.W. Yu, Y.X. Wei, Z.M. Liu, Angew. Chem. Int. Ed. 56 (2017) 9039–9043.
- [7] X.Q. Wu, S.T. Xu, Y.X. Wei, W.N. Zhang, J.D. Huang, S.L. Xu, Y.L. He, S.F. Lin, T.T. Sun, Z.M. Liu, ACS Catal. 8 (2018) 7356–7361.
- [8] J.Z. Li, Y.X. Wei, J.R. Chen, P. Tian, X. Su, S.T. Xu, Y. Qi, Q.Y. Wang, Y. Zhou, Y.L. He, Z.M. Liu, J. Am. Chem. Soc. 134 (2012) 836–839.
- [9] S.T. Xu, A.M. Zheng, Y.X. Wei, J.R. Chen, J.Z. Li, Y.Y. Chu, M.Z. Zhang, Q.Y. Wang, Y. Zhou, J.B. Wang, F. Deng, Z.M. Liu, Angew. Chem. Int Ed. 52 (2013) 11564–11568.
- [10] J.Z. Li, Y.X. Wei, S.T. Xu, P. Tian, J.R. Chen, Z.M. Liu, Catal. Today 226 (2014) 47–51.
- [11] J.F. Haw, W.G. Song, D.M. Marcus, J.B. Nicholas, Acc. Chem. Res. 36 (2003) 317–326.
   [12] U. Olsbye, S. Svelle, K.P. Lillerud, Z.H. Wei, Y.Y. Chen, J.F. Li, J.G. Wang, W.B. Fan, Chem. Soc. Rev. 44 (2015) 7155–7176.
- [13] N. Nesterenko, J. Aguilhon, P. Bodart, D. Minoux, J.P. Dath, in: Zeolites and Zeolite-Like Materials, Elsevier, Amsterdam, 2016, pp. 189–263.
- [14] I. Yarulina, A.D. Chowdhury, F. Meirer, B.M. Weckhuysen, J. Gascon, Nature Catal. 1 (2018) 398–411.
- [15] S. Ilias, A. Bhan, ACS Catal. 3 (2013) 18–31.
- [16] W.N. Zhang, Y.C. Zhi, J.D. Huang, X.Q. Wu, S. Zeng, S.T. Xu, A.M. Zheng, Y.X. Wei, Z.M. Liu, ACS Catal. 9 (2019) 7373-7379.
- [17] M. Dusselier, M.E. Davis, Chem. Rev. 118 (2018) 5265-5329.
- [18] Y.C. Zhi, H. Shi, L.Y. Mu, Y. Liu, D.H. Mei, D.M. Camaioni, J.A. Lercher, J. Am. Chem. Soc. 137 (2015) 15781–15794.
- [19] B. Smit, T.L.M. Maesen, Nature 451 (2008) 671–678.
- [20] U. Olsbye, S. Svelle, M. Bjorgen, P. Beato, T.V. Janssens, F. Joensen, S. Bordiga, K.P. Lillerud, Angew. Chem. Int. Ed. 51 (2012) 5810-5831.
- [21] S. Teketel, M.W. Erichsen, F.L. Bleken, S. Svelle, K. Petter, Catalysis 26 (2014) 179–217.
- [22] J.R. Chen, J.Z. Li, Y.X. Wei, C.Y. Yuan, B. Li, S.T. Xu, Y. Zhou, J.B. Wang, M.Z. Zhang, Z.M. Liu, Catal. Comm. 46 (2014) 36–40.
- [23] J.Z. Li, Y.X. Wei, J.R. Chen, S.T. Xu, P. Tian, X.F. Yang, B. Li, J.B. Wang, Z.M. Liu, ACS Catal. 5 (2015) 661–665.
- [24] W.N. Zhang, J.R. Chen, S.T. Xu, Y.Y. Chu, Y.X. Wei, Y.C. Zhi, J.D. Huang, A.M. Zheng, X.Q. Wu, X.J. Meng, F.S. Xiao, F. Deng, Z.M. Liu, ACS Catal. 8 (2018) 10950–10963.
- [25] P. Ferri, C.G. Li, C. Paris, A. Vidal-Moya, M. Moliner, M. Boronat, A. Corma, ACS Catal. 9 (2019) 11542-11551.
- [26] P. Ferri, C.G. Li, R. Millán, J. Martínez-Triguero, M. Moliner, M. Boronat, A. Corma, Angew. Chem. Int. Ed. 44 (2020) 19708–19715.
- [27] Y. Kumita, J. Gascon, E. Stavitski, J.A. Moulijn, F. Kapteijn, Appl. Catal. A Gen. 391 (2011) 234–243.

- J. Zhong et al./Journal of Catalysis 396 (2021) 23-31 [28] R.L. Smith, S. Svelle, P. Campo, T. Fuglerud, B. Arstad, A. Lind, S. Chavan, M.P. Attfield, D. Akporiaye, M.W. Anderson, Appl. Catal. A Gen. 505 (2015) 1–7. [29] I. Pinilla-Herrero, U. Olsbye, C. Márquez-Álvarez, E. Sastre, J. Catal. 352 (2017) 191–207. [30] I. Pinilla-Herrero, C. Márquez-Álvarez, E. Sastre, Catal. Sci. Tech. 7 (2017) 3892–3901. [31] M.A. Deimund, J.E. Schmidt, M.E. Davis, Top. Catal. 58 (2015) 416-423. [32] Y. Bhawe, M. Moliner-Marin, J.D. Lunn, Y. Liu, A. Malek, M.E. Davis, ACS Catal. 2 (2012) 2490–2495.
  [33] J.H. Kang, R. Walter, D. Xie, T. Davis, C.-Y. Chen, M.E. Davis, S.I. Zones, ChemPhysChem. 19 (2018) 412–419. [34] J.H. Kang, F.H. Alshafei, S.I. Zones, M.E. Davis, ACS Catal. 7 (2019) 6012–6019. [35] M. Yang, B. Li, M.B. Gao, S.F. Lin, Y. Wang, S.T. Xu, X.B. Zhao, P. Guo, Y.X. Wei, M. Ye, P. Tian, Z.M. Liu, ACS Catal. 10 (2019) 3741-3749. [36] J. Kärger, ChemPhysChem 16 (2015) 24-51. [37] R. Krishna, Chem. Soc. Rev. 41 (2012) 3099-3118. [38] S.S. Gao, Z.Q. Liu, S.T. Xu, A.M. Zheng, P.F. Wu, B. Li, X.S. Yuan, Y.X. Wei, Z.M. Liu, J. Catal. 377 (2019) 51-62. [39] N. Wang, Y.C. Zhi, Y.X. Wei, W.N. Zhang, Z.Q. Liu, J.D. Huang, T.T. Sun, S.T. Xu, S.F. Lin, Y.L. He, A.M. Zheng, Z.M. Liu, Nat. Commun. 11 (2020) 1079. [40] S. Svelle, F. Joensen, J. Nerlov, U. Olsbye, K.P. Lillerud, S. Kolboe, M. Bjorgen, J. Am. Chem. Soc. 128 (2006) 14770–14771. [41] M. Bjørgen, S. Svelle, F. Joensen, J. Nerlov, S. Kolboe, F. Bonino, L. Palumbo, S. Bordiga, U. Olsbye, J. Catal. 249 (2007) 195–207. [42] S. Teketel, U. Olsbye, K.P. Lillerud, P. Beato, S. Svelle, Microp. Mesop. Mater. 136 (2010) 33-41. [43] J.Z. Li, Y.X. Wei, Y. Qi, P. Tian, B. Li, Y.L. He, F.X. Chang, X.D. Sun, Z.M. Liu, Catal. Today 164 (2011) 288–292. [44] J.Z. Li, Y.X. Wei, G.Y. Liu, Y. Qi, P. Tian, B. Li, Y.L. He, Z.M. Liu, Catal. Today 171 (2011) 221–228. [45] J.B. Wang, Y.X. Wei, J.Z. Li, S.T. Xu, W.N. Zhang, Y.L. He, J.R. Chen, M.Z. Zhang, A.M. Zheng, F. Deng, X.W. Guo, Z.M. Liu, Catal. Sci. Tech. 6 (2016) 89–97.
   [46] S. Teketel, W. Skistad, S. Benard, U. Olsbye, K.P. Lillerud, P. Beato, S. Svelle, ACS Catal. 2 (2012) 26–37. [47] S. Teketel, L.F. Lundegaard, W. Skistad, S.M. Chavan, U. Olsbye, K.P. Lillerud, P. Beato, S. Svelle, J. Catal. 327 (2015) 22–32. [48] M. Yoshioka, T. Yokoi, T. Tatsumi, ACS Catal. 5 (2015) 4268-4275. [49] S. Park, Y. Watanabe, Y. Nishita, T. Fukuoka, S. Inagaki, Y. Kubota, J. Catal. 319 (2014) 265–273. [50] S. Park, S. Inagaki, Y. Kubota, Catal. Today 265 (2016) 218–224. [51] X.B. Zhao, L.Y. Wang, J.Z. Li, S.T. Xu, W.N. Zhang, Y.X. Wei, X.W. Guo, P. Tian, Z.M. Liu, Catal. Sci. Tech. 7 (2017) 5882-5892. [52] X.B. Zhao, L.Y. Wang, P. Guo, N.N. Yan, T.T. Sun, S.F. Lin, X.W. Guo, P. Tian, Z.M. Liu, Catal. Sci. Tech. 8 (2018) 2966–2974. [53] D. Chen, K. Moljord, T. Fuglerud, A. Holmen, Microp. Mesop. Mater. 29 (1999) 191–203. [54] P. Barger, Methanol to Olefins (MTO) and Beyond, in: M. Guisnet, J.P. Gilson (Eds.), Zeolites for cleaner technologies, Imperial College Press London, 2002, pp. 239–260. [55] D. Chen, A. Grlnvold, K. Moljord, A. Holmen, Ind. Eng. Chem. Res. 46 (2007) 4116–4123. [56] B.P.C. Hereijgers, F. Bleken, M.H. Nilsen, S. Svelle, K.P. Lillerud, M. Bjorgen, B.M. Weckhuysen, U. Olsbye, J. Catal. 264 (2009) 77-87. [57] D. Chen, K. Moljord, A. Holmen, Microp. Mesop. Mater. 164 (2012) 239–250. [58] W.G. Song, H. Fu, J.F. Haw, J. Am. Chem. Soc. 123 (2001) 4749–4754. [59] Y.J. Jiang, J. Huang, V.R. Reddy Marthala, Y.S. Ooi, J. Weitkamp, M. Hunger, Microp. Mesop. Mater. 105 (2007) 132-139. [60] D. Mores, E. Stavitski, M.H.F. Kox, J. Kornatowski, U. Olsbye, B.M. Weckhuysen, Chem. J. Eur. J. 14 (2008) 11320-11327. [61] S.S. Gao, S.T. Xu, Y.X. Wei, Q.L. Qiao, Z.C. Xu, X.Q. Wu, M.Z. Zhang, Y.L. He, S.T. Xu, Z.M. Liu, J. Catal. 367 (2018) 306–314. [62] J.F. Han, Z.Q. Liu, H. Li, J.W. Zhong, J.D. Huang, A.M. Zheng, Y.X. Wei, Z.M. Liu, ACS. Catal. 10 (2020) 8727-8735. [63] M.B. Gao, H. Li, M. Yang, S.S. Gao, P.F. Wu, P. Tian, S.T. Xu, M. Ye, Z.M. Liu, Comm. Chem. 2 (2019) 43–52.
   [64] M.B. Gao, H. Li, W.J. Liu, Z.C. Xu, S.C. Peng, M. Yang, M. Ye, Z.M. Liu, Nat. Comm. 11 (2020) 3641. [65] P. Cnudde, R. Demuynck, S. Vandenbrande, M. Waroquier, G. Sastre, V.V. Speybroeck, J. Am. Chem. Soc. 142 (2020) 6007-6017. [66] W.G. Song, J.F. Haw, Angew. Chem. Int. Ed. 42 (2003) 892–894. [67] J.W. Zhong, J.F. Han, Y.X. Wei, S.T. Xu, Y.L. He, Y.J. Zheng, M. Ye, X.W. Guo, C.S. Song, Z.M. Liu, Chem. Comm. 54 (2018) 3146-3149. [68] J.W. Zhong, J.F. Han, Y.X. Wei, S.T. Xu, T.T. Sun, S. Zeng, X.W. Guo, C.S. Song, Z.M. Liu, Chinese J. Catal. 40 (2019) 477-485. [69] J.W. Zhong, J.F. Han, Y.X. Wei, S.T. Xu, T.T. Sun, X.W. Guo, C.S. Song, Z.M. Liu, Chinese J. Catal. 39 (2018) 1821–1831. [70] J.W. Zhong, J.F. Han, Y.X. Wei, S.T. Xu, T.T. Sun, X.W. Guo, C.S. Song, Z.M. Liu, J. Energ. Chem. 5 (2019) 174-181. [71] H.W. Huang, H.R. Wang, H. Zhu, S.H. Zhang, Q. Zhang, C.Y. Li, Catal. Sci. Tech. 9 (2019) 2203–2210.
   [72] H.W. Huang, M.Y. Yu, Q. Zhang, C.Y. Li, Microp. Mesop. Mater. 295 (2020) 109971.
- [73] S.C. Peng, M.B. Gao, H. Li, M. Yang, M. Ye, Z.M. Liu, Angew. Chem. Int. Ed. (2020), https://doi.org/10.1002/anie.202009230.
- [74] J.B. Zhou, Y.C. Zhi, J.L. Zhang, Z.Q. Liu, T. Zhang, Y.L. He, A.M. Zheng, M. Ye, Y.X. Wei, Z.M. Liu, J. Catal. 377 (2019) 153–162.
- [75] W. Zhou, K. Chin, J. Zhang, C. Zhou, V. Subramanian, Q.H. Zhang, Y. Wang, Chem. Soc. Rev. 48 (2019) 3193–3228.
   [76] A. Dokania, A. Ramirez, A. Bavykina, J. Gascon, ACS Energy Lett. 4 (2019) 167–176.
- [77] F. Jiao, J.J. Li, X.L. Pan, J.P. Xiao, H.B. Li, H. Ma, M.M. Wei, Y. Pan, Z.Y. Zhou, M.R. Li, S. Miao, J. Li, Y.F. Zhu, D. Xiao, T. He, J.H. Yang, F. Qi, Q. Fu, X.H. Bao, Science 351 (2016) 1065-1068.
- [78] Y.M. Ni, Y. Liu, Z.Y. Chen, M. Yang, H.C. Liu, Y.L. He, Y. Fu, W.L. Zhu, Z.M. Liu, ACS Catal. 9 (2) (2019) 1026-1032.
- [79] K. Cheng, B. Gu, X.L. Liu, J.C. Kang, Q.H. Zhang, Y. Wang, Angew. Chem. Int. Ed. 55 (2016) 4725–4728.
- [80] X.L. Liu, W. Zhou, Y.D. Yang, K. Cheng, J.C. Kang, L. Zhang, X.J. Min, Q.H. Zhang, Y. Wang, Chem. Sci. 9 (2018) 4708–4718.
   [81] Z.L. Li, J.J. Wang, Y.Z. Qu, H.L. Liu, C.Z. Tang, S. Miao, Z.C. Feng, H.Y. An, C. Li, ACS Catal. 7 (2017) 8544–8548.
- [82] P. Gao, S.S. Dang, S.G. Li, X.N. Bu, Z.Y. Liu, M.H. Qiu, C.G. Yang, H. Wang, L.S. Zhong, Y. Han, Q. Liu, W. Wei, Y.H. Sun, ACS Catal. 8 (2018) 571-578.